58-12-89 [redacted] MAR 3 1 1958 10692 Copy 228
RM L58A13

NACA RM L58A13

TECHNICAL LIBRARY
AFL 2291

TECH LIBRARY KAFB, NM
0144745

7829

NACA

RESEARCH MEMORANDUM

HEAT TRANSFER TO 0° AND 75° SWEPT BLUNT LEADING EDGES IN FREE FLIGHT AT MACH NUMBERS FROM 1.90 TO 3.07

By Robert L. O'Neal and Aleck C. Bond

Langley Aeronautical Laboratory
Langley Field, Va.

Classification cancelled (~~or changed to~~ Unclassified)
Authority of NASA TECH Pub (OFFICER AUTHORIZED TO CHANGE)
By ANNOUNCEMENT No 48 22 June 1961
NAME AND
Sidney Hodges
DATE 7 July 1961

[redacted]

NATIONAL ADVISORY COMMITTEE
FOR AERONAUTICS
WASHINGTON
March 24, 1958

[redacted]

AFMDC ADJ '58-2179

TECH LIBRARY KAFB, NM
0144745

 [redacted]

NATIONAL ADVISORY COMMITTEE FOR AERONAUTICS

RESEARCH MEMORANDUM

HEAT TRANSFER TO 0° AND 75° SWEPT BLUNT LEADING EDGES IN FREE FLIGHT AT MACH NUMBERS FROM 1.90 TO 3.07

By Robert L. O'Neal and Aleck C. Bond

SUMMARY

A flight investigation of a rocket-powered model was conducted to study the heat transfer to wing leading edges in the vicinity of their juncture with a cylindrical body. Heat-transfer data were obtained on leading edges of $\frac{3}{4}$-inch diameter at sweep angles of 0° and 75°, Mach numbers from 1.90 to 3.07, and Reynolds numbers based on leading-edge diameter from 8.05×10^5 to 11.80×10^5. The measured heating rates of both the 0° and 75° swept leading edges were of the magnitude predicted by turbulent theory rather than by laminar theory. It is believed that the high level of heating observed on the leading edges was due to the influence of conditions existing in the turbulent boundary layer of the body. Comparison of the average measured heating on the cylindrical portions of both the swept and unswept leading edges indicates that the heating of the unswept segment was generally about twice that of the swept segment.

INTRODUCTION

As a result of current interest in the flight of aircraft at both supersonic and hypersonic speeds, considerable research, both theoretical and experimental, has been stimulated in the problem of the aerodynamic heating of wing leading edges. (See, for example, refs. 1 to 6.) The experimental data of references 4 and 5, which deal with the effect of sweep on leading-edge heating, were obtained at relatively low values of stream Reynolds number and the results were shown to be generally in good agreement with theories for a laminar boundary layer. The experiments of reference 6 which were conducted at considerably larger values of stream Reynolds number, however, indicated large increases in heat transfer with increase in yaw angle which, apparently, were caused by transition from laminar to turbulent boundary layer.

[redacted]

AFMDC ADJ '58-2179

As part of the effort to provide further insight into the problem of aerodynamic heating of wing leading edges at conditions of high speed and large Reynolds numbers, a rocket-powered-model test was conducted at the Langley Pilotless Aircraft Research Station at Wallops Island, Va. for the purpose of measuring the heat transfer to swept and unswept blunt leading edges. Measurements were made in the vicinity of the wing-body juncture where the aerodynamic heating is critical. Leading-edge segments of sufficient diameter to give Reynolds numbers representative of full scale and to allow measurements of local heating were utilized. Heat-transfer data were obtained on wing segments having cylindrical leading edges of $\frac{3}{4}$-inch diameter and sweep angles of 0° and 75° for a Mach number range from 1.90 to 3.07 and Reynolds number based on leading-edge diameter from 8.05×10^5 to 11.80×10^5.

SYMBOLS

A	area, sq ft
C_p	pressure coefficient, $\dfrac{P_l - P_\infty}{0.7P_\infty M^2}$
C	distance along chord, perpendicular to leading edge, in.
c_p	specific heat of air at constant pressure, Btu/lb-$^{\circ}$F
c_w	specific heat of wall material, Btu/lb-$^{\circ}$F
D	leading-edge diameter, ft
g	gravitational constant, 32.2 ft/sec^2
h	local aerodynamic heat-transfer coefficient, Btu/(sq ft)(sec)($^{\circ}$F)
k	thermal conductivity of wall material, Btu-ft/(sq ft)(sec)($^{\circ}$F)
M	Mach number
N_{St}	Stanton number, $h/gc_p\rho_\infty V_\infty$
$\bar{N}_{St}$	average Stanton number, $h_{average}/gc_p\rho_\infty V_\infty$

P	pressure, lb/sq ft
N_{Pr}	Prandtl number
Q	quantity of heat per unit time, Btu/sec
q	heating rate, Btu/(sq ft)(sec)
R_D	Reynolds number based on leading-edge diameter and free-stream conditions
S	distance measured along segment wall perpendicular to leading edge, ft
T	temperature, $^{\circ}F$
t	time, sec
V	velocity, ft/sec
Λ	leading-edge sweep angle, deg
Φ	azimuth angle measured from forward stagnation point perpendicular to leading edge, deg (see figs. 3 and 4)
μ	viscosity of air, slugs/ft-sec
ρ	density of air, slugs/cu ft
ρ_w	density of wall material, lb/cu ft
τ	thickness of wall, ft
c_f	local skin-friction coefficient

Subscripts:

aw	adiabatic wall
l	local conditions just outside boundary layer
s	outside surface of wall
t	stagnation conditions

[redacted]

w wall conditions

∞ undisturbed free stream ahead of model

MODEL, INSTRUMENTATION, AND TEST

The vehicle employed for the test was a body of revolution consisting of an ogive-cylinder-flare configuration. Four small wing segments representing portions of the leading edges of 0° and 75° swept wings were symmetrically mounted 90° apart at zero incidence on the cylindrical portion of the vehicle as shown in the sketch of figure 1 and photograph of figure 2.

The leading-edge segments had cylindrical leading edges of $\frac{3}{4}$-inch diameter which became tangent to flat surfaces inclined at 4.27° to the chord plane (see fig. 3). The wall thickness as measured with a micrometer at several locations on each leading-edge segment was found to be 0.0625 inch. A resin material was used to close off the tips and trailing edges of the segments to protect the interior from the airstream. The outside surface of each leading-edge segment was oxidized to provide a surface with a stabilized emissivity. The surface roughness of the oxidized surfaces was not measured; however, from previous experience it is estimated that the roughness was of the order of 15 to 20 microinches.

One unswept segment and one swept leading-edge segment were provided with chromel-alumel thermocouples spotwelded to the inside surface of the leading edges. Four temperature measurements were made on the unswept segment and six on the swept segment with the thermocouples being located as shown in figure 3. Local surface pressures were measured only on the duplicate unswept segment and the orifices were located as shown in figure 4.

The test vehicle was instrumented with an NACA eight-channel telemeter which transmitted leading-edge temperature and pressure data and vehicle acceleration data to a ground receiving station. Details of the thermocouple telemetering technique employed may be found in reference 7.

Other instrumentation included a CW Doppler radar which provided measurements of model velocity and an NACA modified SCR-584 radar which provided data for obtaining the position of the model in space. Atmospheric data and wind conditions were determined by means of a radiosonde launched near the time of flight and tracked by a Rawin set AN/GMD-1A.

The test vehicle and boosters are shown on the launcher in figure 5. The propulsion system consisted of three stages of solid propellant rocket motors. The first stage was an M5 JATO rocket motor and the second and third stages were JATO, 6-KS-3000, T40 and JATO, 1.3-KS-4800, T-55 rocket motors, respectively.

The propulsion system for the test had been selected to give a calculated peak speed of about $M = 7.5$ occurring at an altitude of about 47,500 feet; however, because of model failure at the end of first-stage burning, data were obtained only to a Mach number of 3.07 at a flight time of 3.3 seconds. Time histories of stream static temperature and pressure as determined from the radiosonde measurements for the model trajectory are shown in figure 6 along with the calculated variation of the flight stagnation temperature. The variation with time of flight Mach number determined from the measured model velocity and the stream Reynolds number based on the leading-edge diameter of 3/4 inch is shown in figure 7. Accelerometer data indicated that the model angle of attack was small (less than 0.50°) during the period for which data are reported and, hence, the effect of angle of attack was ignored in the reduction and analysis of the data.

DATA REDUCTION

Local Flow Conditions

Local flow conditions existing just outside the boundary layer on the unswept leading-edge segment were calculated from measured pressure data. Local pressures were measured in flight on the unswept leading-edge segment at the locations indicated in figure 4 and are plotted as pressure coefficients in figure 8. The measured values of local pressure were used to obtain local Mach numbers and temperatures by assuming isentropic expansion back from the stagnation point. The local conditions for station $C = 0.50$ were assumed to be the same as those obtained by this procedure for station $C = 1.00$.

No pressure measurements were made in flight on the 75° swept leading-edge segment; however, local pressures were calculated by use of unswept-segment pressure data. This calculation was made by considering the airstream to be two components of flow, one tangential and one normal to the leading edge of the swept segment. It was assumed that pressures on the segment were not affected by the tangential component of flow but were due entirely to the component of flow normal to the leading edge. This normal component of flow was $M_N = M_{\infty} \cos 75^{\circ}$. It was also assumed that local pressure coefficients based on this normal component of Mach number (and dynamic pressure based on this Mach number)

were equal to pressure coefficients measured on the unswept segment at a free-stream Mach number equal to this normal component. With the use of the local pressures obtained from these pressure coefficients, the component of the local Mach number normal to the leading edge was obtained by assuming isentropic expansion back from the stagnation point in a direction perpendicular to the leading edge. This normal component was added vectorially to the tangential component obtained from the relation $M_t = M_\infty \sin 75^\circ$ to give values of local Mach number. The values of local Mach number were then used to obtain local temperatures. The use of the relation $M_t = M_\infty \sin 75^\circ$ for obtaining local tangential Mach number is justified since the resulting local temperatures were of the same order as the free-stream static temperatures.

A check of this method of determining the swept-segment local stagnation-line pressures was afforded by the data of reference 8. The pressure coefficient determined for the stagnation line of the 75° swept segment at a stream Mach number of 1.98 was compared with the reported cylinder pressure coefficients (ref. 8) for an angle of attack of 15°. The value of pressure coefficient of 0.068 thus determined showed good agreement with the experimental data of reference 8.

As adiabatic wall temperature is a weak function of local temperature, it is not necessary that local temperatures be known precisely to obtain reasonable accuracy in calculated heat-transfer coefficients. For this investigation a change of 10 percent in local temperature causes less than a 2-percent change in free-stream Stanton number. It was believed that pressure coefficients obtained from unswept-segment data would yield local temperatures within a 10-percent accuracy and were thus sufficiently accurate for evaluating Stanton number based on free-stream conditions. The estimated maximum probable error in the measured wall temperatures was about 18°. Calculations using estimated errors in the various quantities involved in obtaining Stanton number indicate that the experimental Stanton numbers presented are accurate to within about 15 percent.

Adiabatic Wall Temperature, Wall Heating Rate, and Heat-Transfer Coefficient

In order to calculate the local values of heat-transfer coefficient, it was necessary to evaluate local adiabatic wall temperatures. At the stagnation point on the 0° swept leading-edge segment the temperature recovery factor was assumed to be unity or $T_{aw} = T_t$.

At the stagnation point on the 75° swept segment the adiabatic wall temperature was obtained by using the expression derived in reference 2 for a yawed cylinder. For a turbulent boundary layer this expression based on free-stream temperature is

$$\frac{T_{aw} - T_\infty}{T_t - T_\infty} = 1 - \left(1 - N_{Pr}^{1/3}\right)\sin^2\Lambda$$

At points other than the stagnation line of both leading-edge segments the relation used for calculating T_{aw} was

$$\frac{T_{aw} - T_l}{T_t - T_l} = N_{Pr}^{1/3}$$

In all cases the Prandtl number was evaluated at the outside surface temperature.

Because of the high heating rates and low thermal conductivity of the test surfaces of this investigation, it was necessary to consider the temperature gradient through the skin before determining actual wall heating rates. The outside-surface temperatures of the leading-edge segments were calculated from the measured time history of the inside-wall temperatures by the method described in the appendix. An average wall-temperature time history was obtained by taking the numerical average of the outside and inside-surface temperatures and plotting this value as a function of time. A smooth curve was faired through the points and the slopes of the tangents to the curve were measured at intervals of 0.10 second. These slopes were plotted against time and a smooth curve was faired through the points. The faired values of the slope $\frac{dT_w}{dt}$ were then used to calculate the wall heating rate by the relation

$$q = \rho_w c_w \tau \frac{dT_w}{dt}$$

where c_w was evaluated at the average wall temperature. This gave the amount of heat per unit area that went into raising the temperature of the skin. Since the temperature distribution through the wall material is not a linear function of thickness, a calculation of the wall heating rates, obtained by using an integrated average wall-temperature history, was made for the stagnation point of the unswept leading-edge segment

for comparison with the heating rates obtained by using the numerical average wall-temperature history. The wall heating rate obtained in this manner was found to differ from the value obtained by using the numerical average wall-temperature history by less than 3 percent at 2.5 seconds. This difference decreased to less than 1 percent at 3.3 seconds.

A calculation was also made to determine the effect of chordwise conduction on the local heat-transfer parameters. It was found that the maximum amount of conduction for both leading-edge segments was a loss of heat from the stagnation points and amounted to 3 percent of the measured heat input rates. Inasmuch as this loss occurred at the highest wall temperature and was considerably less at the lower wall temperatures, no corrections to the local heat-transfer data were made. The amount of heat lost by radiation was calculated and found to be negligible at all surface temperatures existing for this flight.

The local heat-transfer coefficients per unit area were calculated by the relation

$$h = \frac{1}{T_{aw} - T_s} \rho_w c_w \tau \frac{dT_w}{dt}$$

where T_s is the calculated outside surface temperature of the wall.

The average heat-transfer coefficients around the cylindrical portion of the leading-edge segments were evaluated graphically by the expression

$$\bar{h} = \frac{1}{0.562} \int_{S=0}^{S=0.562} h_{local}\, dS$$

The limit $S = 0.562$ is the arc length from the stagnation point to the tangent of the cylinder with the flat portion.

RESULTS AND DISCUSSION

Pressure Distribution

Pressure coefficients measured on the unswept leading-edge segment are shown in figure 8. Pitot pressure coefficients were calculated for the flight conditions and are also shown in figure 8. At values of t

before $t = 1.0$ second, the experimental stagnation-pressure coefficients are somewhat lower than the pitot pressure coefficients. It is possible that this disagreement was caused by separation occurring on the body and influencing the pressure on the wing in the region where pressure measurements were made. Although measured stagnation-pressure coefficients in the time range from $t = 1.0$ to $t = 2.5$ seconds are higher than pitot pressure coefficients, they are at all points within 10 percent of the stagnation-pressure coefficient which could exist if an oblique shock wave were present in front of the leading edge. The negative pressure coefficients measured on the flat portion of the leading-edge segment at the earlier times indicate overexpansion of the air around the leading edge with the sharp rise in the curve probably being caused by the flow becoming supersonic at this time.

The method of relating local pressures to the 75° swept leading-edge segment as described in the section entitled "Data Reduction" may not be precisely correct inasmuch as the flow over this swept segment is probably three dimensional. It is believed, however, that local temperatures obtained by using these pressures on the swept segment are sufficiently accurate to evaluate local adiabatic wall temperature. The pressures which were applied to the swept segment are in the time range from 0.70 to 1.06 seconds.

Skin Temperatures

The relatively high heating rates of this investigation and low thermal conductivity of the leading-edge material made the temperature gradient through the skin of such magnitude that it had to be considered in order to determine accurately the heat transfer. Outside-surface temperatures calculated by the method described in the appendix are shown in figures 9 and 10 along with the measured inside-surface temperatures. The calculations of the outside-surface temperatures were started at $t = 1.6$ seconds. Skin temperatures and heat-transfer data are not presented for values of t below 2.2 seconds inasmuch as the skin-temperature variation with time was not of sufficient magnitude to determine the wall heating rates accurately. Calculated outside-surface temperatures for each thermocouple on both the 0° and 75° swept segments are shown as a function of S/D for various free-stream Mach numbers in figure 11. The dashed portion of the curves for the 75° swept segment indicates that the thermocouple at the most rearward station was not in the same chordwise plane as the measurements indicated by the solid curve. As expected, the temperature at the stagnation point on the unswept leading-edge segment is higher in all cases than at the corresponding point on the 75° swept segment. The temperature of both segments decreases with increasing chordwise distance and the effects of sweep angle become less pronounced with increasing chordwise distance.

HEAT TRANSFER

Heat-Transfer Measurements

The heat-transfer data are presented as nondimensional Stanton number evaluated at free-stream conditions. The Stanton number was evaluated at free-stream conditions rather than at local conditions inasmuch as it was felt that local flow conditions on the 75° swept segment were not known precisely enough for this use.

Stanton number for each thermocouple location is shown as a function of time in figure 12 for both leading-edge segments. Data are shown for both inboard and outboard stations at two chordwise locations on the 75° swept segment. The deviation between the heating data at the two stagnation points and at the two $\Phi = 45^{\circ}$ points from their respective mean values is within the quoted experimental accuracy of these data.

Average Heat Transfer on Cylindrical Portions of Leading Edges

An approximation of the average Stanton number for the cylindrical portions of the leading edges was obtained by integrating the curve passing through the limited measurements of the local Stanton number. These values for both the 0° and 75° leading-edge segments are shown as a function of time in figure 13 and are compared with the theoretical average heating with a laminar boundary layer. Values of the theoretical average heating were obtained by integrating local values of heat transfer obtained by using the theory of reference 4. Since these experimental data were so much higher than the values predicted by laminar theory, it was believed that the boundary layer over the leading edges was of a turbulent nature. In order to investigate this eventuality the approximate theory proposed by Beckwith (ref. 6) was used to evaluate the theoretical average turbulent heat transfer for the unswept leading-edge segment. Comparison of this theoretical prediction with the measured average Stanton numbers for the unswept segment is made in figure 13(a), and it is seen that the data show reasonably good agreement with the theoretical curve after a time of about 2.6 seconds. Prior to 2.6 seconds it appears that the flow on the unswept segment was of a transitional nature.

Since Beckwith's approximate theory is limited to cases for which the Mach number component normal to the leading edge is supersonic, another approach had to be resorted to for evaluating the theoretical average turbulent heat transfer for the 75° swept leading-edge segment.

This consisted simply of the evaluation of the local turbulent flat-plate heat-transfer coefficient, around the cylindrical portion of the leading edge, for the calculated local streamwise-flow conditions and integration of the resulting distribution for an average value. Heat-transfer coefficients for a flat plate with a turbulent boundary layer were obtained from references 9 and 10 with a value of 0.6 being assumed for the ratio of Stanton number to skin-friction coefficient. Local pressures for the swept leading edge were obtained from faired pressure distributions, determined from the unswept experimental pressure data as explained in the section entitled "Data Reduction." Local flow conditions were estimated by use of these pressure data in conjunction with the total pressure resulting behind an oblique shock induced by a conical surface with a 15° semivertex angle. The streamwise distance from the stagnation point to the point in question was used for calculating the local Reynolds number. A comparison of the measured average Stanton numbers for the 75° swept leading edge with this theoretical average turbulent prediction is also included in figure 13(b), and it is seen that the agreement is quite good. The fact that the average data for the cylindrical portions of both the 0° and 75° swept segments agree so well with the theoretical predictions for a turbulent boundary layer substantiates the fact that the flow over the leading edges was turbulent. Comparison of the average measured heating on the swept and unswept leading edges (fig. 13) indicates that after 2.6 seconds the heating of the unswept segment is about twice that of the swept segment.

Local Heat Transfer

The experimental heat-transfer data for the two measuring stations on the flat portion of the unswept leading-edge segment are shown in figures 14(a) and 14(b) and are compared with predicted values of both laminar and turbulent flat-plate theories. The laminar theory used is that found in reference 11 and the turbulent predictions were obtained by using the Van Driest theory (refs. 9 and 10) with a value of 0.6 being assumed for the ratio of Stanton number to skin-friction coefficient. Except for the interval between 2.2 to 2.5 seconds for the forward measuring point (C = 0.50 in.) this comparison (fig. 14(a)) shows very good agreement between the data of both measuring points and the predictions of the turbulent flat-plate theory and lends further credence to the fact that the flow over the cylindrical portion of this segment was turbulent. In the interval from 2.2 to 2.5 seconds the comparison shows transitional flow at the forward measuring point (C = 0.50 in.) which is compatible with the interval of transitional flow on the cylindrical portion of the segment, observed from the data of figure 13(a). The experimental heat-transfer data for the two measuring stations on the flat portion of the 75° swept leading-edge segment are shown in figures 14(c) and 14(d) and are compared with the heat

transfer predicted by laminar and turbulent flat-plate theories. The theories are the same ones used for the unswept segment with the streamwise distance from the stagnation point to the station in question being used for calculating the local Reynolds number. The experimental heat-transfer data at station $C = 0.50$ inch are somewhat lower than the values predicted by turbulent theory, while good agreement is shown between experiment and turbulent theory at station $C = 1.00$ inch.

The experimental heating data are summarized in figure 15 by replotting the experimental Stanton numbers as a function of the nondimensional distance S/D for several times of the flight test. Determination of the local theoretical values shown has been previously discussed with the exception of the theoretical turbulent heating of the cylindrical portion of the unswept leading edge. These values were obtained in the same manner as were the turbulent predictions for the cylindrical portion of the swept leading edge - that is, the evaluation of the local turbulent flat-plate heat transfer corresponding to the calculated local conditions. For the purpose of clarity the theoretical predictions are shown as bands rather than the individual curves for each particular time, with each band being determined by the extreme values predicted for the range of time from 2.20 to 3.30 seconds. In figure 15(a) it is clearly seen that the measured data for the unswept segment are considerably higher than the predictions of the laminar theory and only at the earlier time of 2.2 seconds does the flow appear to have been transitional on the forward part of the segment. The measured stagnation-point values which would ordinarily be expected to agree with the predictions of laminar theory are generally about twice as great as the laminar theory. Comparison of the measured cylinder values with the predictions of the flat-plate theory does not afford very good correlation with regard to the individual values, possibly because of the extension of the theory beyond its intended usage. However, it is interesting to note that the average heat transfer to the cylinder would be predicted fairly well by this theory, at least for this case. In figure 15(b) the experimental data for the 75° swept segment are shown to be of a turbulent level at all times for which the data are presented. The measured stagnation-point values are of the order of three times as great as those predicted by laminar theory. There is generally good agreement between the turbulent theory and experiment in both trend and magnitude. It is worthy of note that the predictions of the flat-plate theory of the heating to the cylindrical portions of the leading edges show much better agreement with experiment in the case of the swept leading edge than in the case of the unswept leading edge.

In view of the results of Beckwith and Gallagher (ref. 6) which showed the effect of yaw angle on boundary-layer transition on cylinders, the higher than laminar level of heating observed on the 75° swept leading-edge segment is not surprising; however, the reason for turbulent

flow over the 0° swept segment is not clear from the limited measurements made on the model. It is believed, however, that, since the measurements were made at a point of only 1.25 inches from the body, the flow on the leading edge could have been influenced by conditions existing in the body boundary layer. For the period of time of the data presentation (2.2 seconds to 3.3 seconds) the Reynolds number for the body at the leading-edge—body juncture varied from 45.51×10^6 to 66.71×10^6 and the body boundary-layer thickness was estimated to range from 0.46 to 0.50 inch. With these conditions prevailing, it is possible that interaction between the bow shock ahead of the leading edge and the thick turbulent boundary layer of the body could have increased the heating rate of the leading edge to the turbulent level.

It is recognized that, because of the large leading-edge diameter and the small span of the leading-edge segments, the flow in the vicinity of a full-scale wing-body juncture may not have necessarily been duplicated by this test. The data do indicate, however, that heat-transfer rates considerably higher than would be encountered by a wing leading edge with laminar flow in an undisturbed flow field are possible in the region of the wing-body juncture.

CONCLUSIONS

A flight investigation has been conducted to study the heat transfer to 0° and 75° swept leading-edge segments in the vicinity of the wing-body juncture. Data were obtained for a Mach number range from 1.90 to 3.07 and for a Reynolds number range based on leading-edge diameter from 8.05×10^5 to 11.80×10^5. The following pertinent conclusions are drawn from the results:

1. Comparison of the average measured heat transfer to the cylindrical portions of both the 0° and 75° swept leading-edge segments with theoretical predictions of the average turbulent heat transfer showed reasonably good agreement; this agreement indicated that the flow on the leading edges was for the most part turbulent. It is believed that the high level of heating observed on the leading edges was due to the influence of conditions existing in the body boundary layer.

2. Comparison of the average measured heat transfer to the 0° and 75° swept leading edges indicates that the heat transfer to the unswept segment was generally about twice that to the swept segment.

3. Measurements at the stagnation points of the leading-edge segments indicated that for the unswept segment the heat transfer was

approximately two times as great and for the 75° swept segment the heat transfer was of the order of three times as great as that predicted by laminar theory.

4. Even though exact simulation of the flow field at the wing-body juncture may not have been provided by the short leading-edge segments, it is felt that the present data do indicate an important problem area and that, further, more complete investigations are needed to understand the heating of leading edges in the vicinity of the wing-body juncture.

Langley Aeronautical Laboratory,
National Advisory Committee for Aeronautics,
Langley Field, Va., January 6, 1958.

APPENDIX

METHOD OF CALCULATING WALL TEMPERATURE GRADIENTS

Outside-surface temperatures of the wing leading-edge segments were calculated from measured inside-surface temperatures by assuming one-dimensional heat conduction through the wall. These calculations were based on the method of Dusinberre as found in reference 12. For the computation of the outside-surface temperatures the wall was analytically divided into a number of elements of equal thickness and heat-balance equations were written for each element. The following sketch shows the elements of a typical cross section of the leading edge:

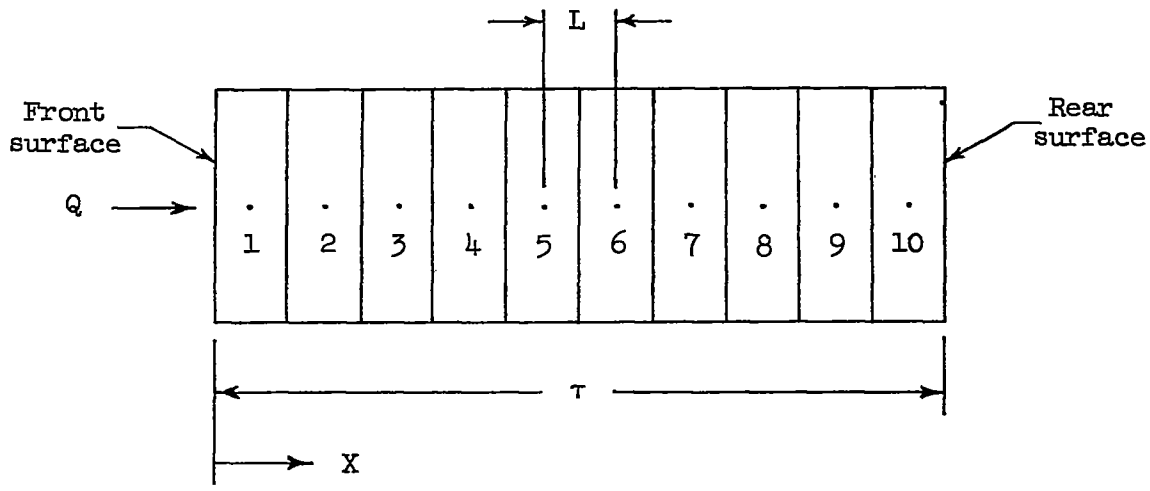

In setting up the heat-balance equations for calculating temperatures the following assumptions are made:

(1) The temperature of each element is uniform.

(2) An element gains heat only by one-dimensional conduction from adjacent elements.

(3) For the inside-surface element the heat gained or lost by radiation and convection is small and, therefore, can be neglected.

The condition stipulated by a heat-balance equation for an element is that the difference between the heat gained and the heat lost by conduction or other means is equal to the heat stored in the element. The heat gained or lost by conduction per unit time is by Fourier's law of one-dimensional heat conduction

$$Q = kA \frac{dT}{dX}$$

and the heat stored in an element per unit time of volume v is

$$Q = v\rho_w c_w \frac{dT}{dt}$$

This gives as a heat-balance equation for a typical element, such as number 5,

$$v\rho_w c_w \frac{dT}{dt} = Q_{in} - Q_{out}$$

or

$$v\rho_w c_w \frac{dT_5}{dt} = \frac{kA\left(T_4 - T_5\right)}{L} + \frac{kA\left(T_6 - T_5\right)}{L}$$

The temperature rise of this element during the time Δt is then

$$\Delta T_5 = \left[\frac{kA\left(T_4 - T_5\right)}{v\rho_w c_w L} + \frac{kA\left(T_6 - T_5\right)}{v\rho_w c_w L}\right]\Delta t$$

This equation can be solved for T_4 and the result is

$$T_4 = \frac{v\rho_w c_w L}{kA\ \Delta t}\Delta T_5 + 2T_5 - T_6$$

where c_w and k are evaluated at T_5. The temperature equation of each element can be written in the same manner:

$$T_{10} = \text{Known}$$

$$T_9 = \frac{v\rho_w c_w L}{kA\ \Delta t}\Delta T_{10} + T_{10}$$

$$T_8 = \frac{v\rho_w c_w L}{kA\ \Delta t}\Delta T_9 + 2T_9 - T_{10}$$

$$\cdot\ \cdot\ \cdot\ \cdot\ \cdot\ \cdot\ \cdot$$

$$T_1 = \frac{v\rho_w c_w L}{kA\ \Delta t}\Delta T_2 + 2T_2 - T_3$$

The values used for inside-surface temperature are average values over the time interval.

As the temperature increases in going from element 10 to element 1, any scatter in the temperature values of element 10 used becomes magnified in the calculated temperatures of the other elements. The amount of scatter that can be tolerated depends on the number of elements into which the wall is divided and on the actual temperature gradient across the wall. For the calculation made for this report it was necessary to use values of T_{10} and ΔT_{10} to the nearest 0.1°. The necessary precision was obtained by plotting T_{10} as a function of time and evaluating ΔT_{10} at intervals of 0.05 second. These values were then plotted as a function of time to a large scale and faired by a smooth curve. The new values of ΔT_{10} were then added successively to the values of T_{10}, starting with the value that exists at the time of zero temperature gradient through the skin. The function $\frac{v\rho_w c_w L}{kA\ \Delta t}$ was expressed as an analytical function of temperature and with the values of T_{10} the temperatures of each element were calculated by an IBM 650 Digital Computer. Figures 9 and 10 show the calculated outside-surface temperatures obtained by using this method.

REFERENCES

1. Reshotko, Eli, and Cohen, Clarence B.: Heat Transfer at the Forward Stagnation Point of Blunt Bodies. NACA TN 3513, 1955.

2. Reshotko, Eli: Heat Transfer to a Yawed Infinite Cylinder in Compressible Flow. 1956 Heat Transfer and Fluid Mechanics Inst. Stanford Univ. (Stanford, Calif.), June 21-23, 1956, pp. 205-220.

3. Beckwith, Ivan E.: Theoretical Investigation of Laminar Heat Transfer on Yawed Infinite Cylinders in Supersonic Flow and a Comparison With Experimental Data. NACA RM L55F09, 1955.

4. Goodwin, Glen, Creager, Marcus O., and Winkler, Ernest L.: Investigation of Local Heat-Transfer and Pressure Drag Characteristics of a Yawed Circular Cylinder at Supersonic Speeds. NACA RM A55H31, 1956.

5. Feller, William V.: Investigation of Equilibrium Temperatures and Average Laminar Heat-Transfer Coefficients for the Front Half of Swept Circular Cylinders at a Mach Number of 6.9. NACA RM L55F08a, 1955.

6. Beckwith, Ivan E., and Gallagher, James J.: Experimental Investigation of the Effect of Boundary-Layer Transition on the Average Heat Transfer to a Yawed Cylinder in Supersonic Flow. NACA RM L56E09, 1956.

7. Rumsey, Charles B., and Lee, Dorothy B.: Measurements of Aerodynamic Heat Transfer and Boundary-Layer Transition on a 15° Cone in Free Flight at Supersonic Mach Numbers Up to 5.2. NACA RM L56F26, 1956.

8. Perkins, Edward W., and Kuehn, Donald M.: Comparison of the Experimental and Theoretical Distributions of Lift on a Slender Inclined Body of Revolution at $M = 2$. NACA TN 3715, 1956.

9. Van Driest, E. R.: The Turbulent Boundary Layer for Compressible Fluids on a Flat Plate With Heat Transfer. Rep. No. AL-997, North American Aviation, Inc., Jan. 27, 1950.

10. Van Driest, E. R.: The Turbulent Boundary Layer With Variable Prandtl Number. Rep. No. AL-1914, North American Aviation, Inc., Apr. 2, 1954.

11. Van Driest, E. R.: Investigation of Laminar Boundary Layer in Compressible Fluids Using the Crocco Method. NACA TN 2597, 1952.

12. McAdams, William H.: Heat Transmission. Third ed., McGraw-Hill Book Co., Inc., 1954, p. 44.

[redacted]

[redacted]

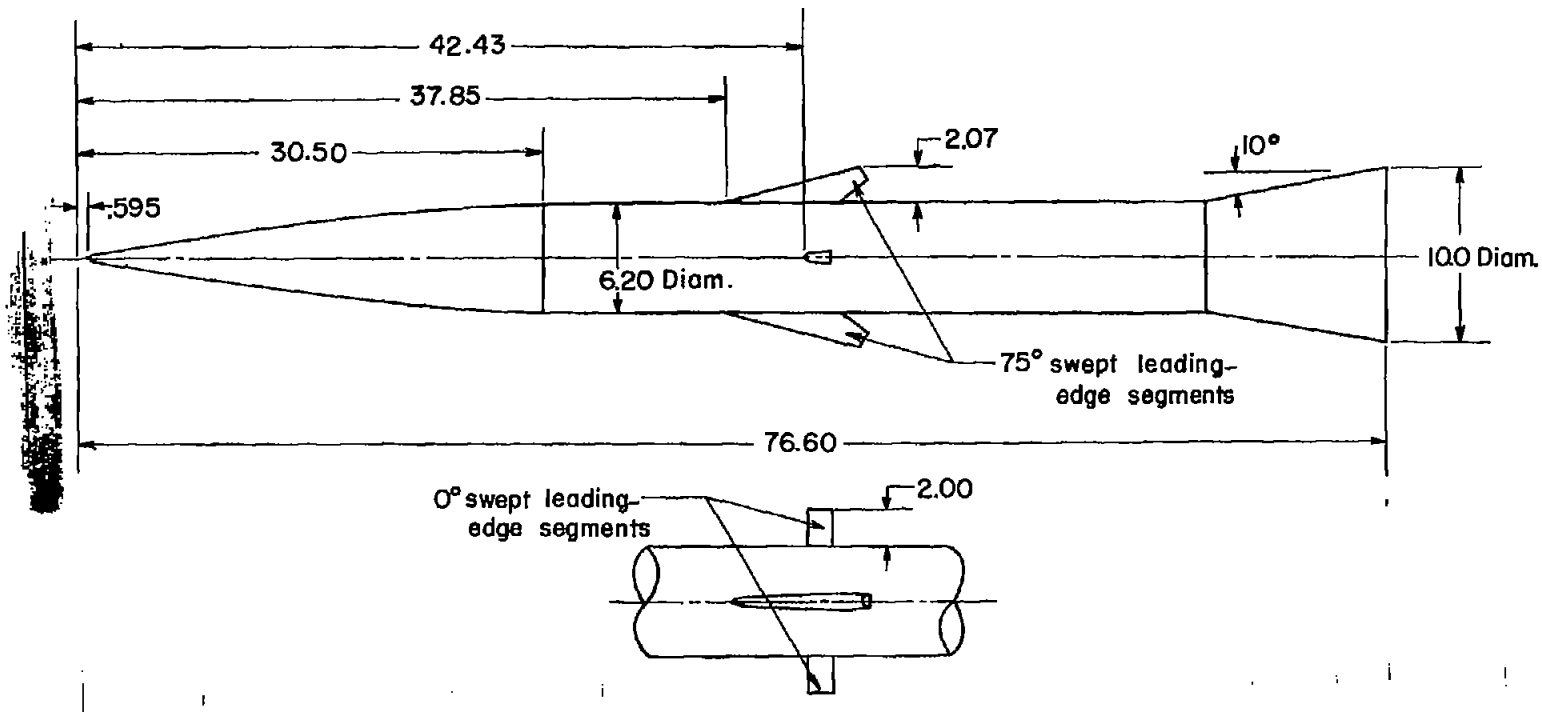

Figure 1.- Sketch of test vehicle showing location of wing leading-edge segments. All dimensions are in inches unless otherwise noted.

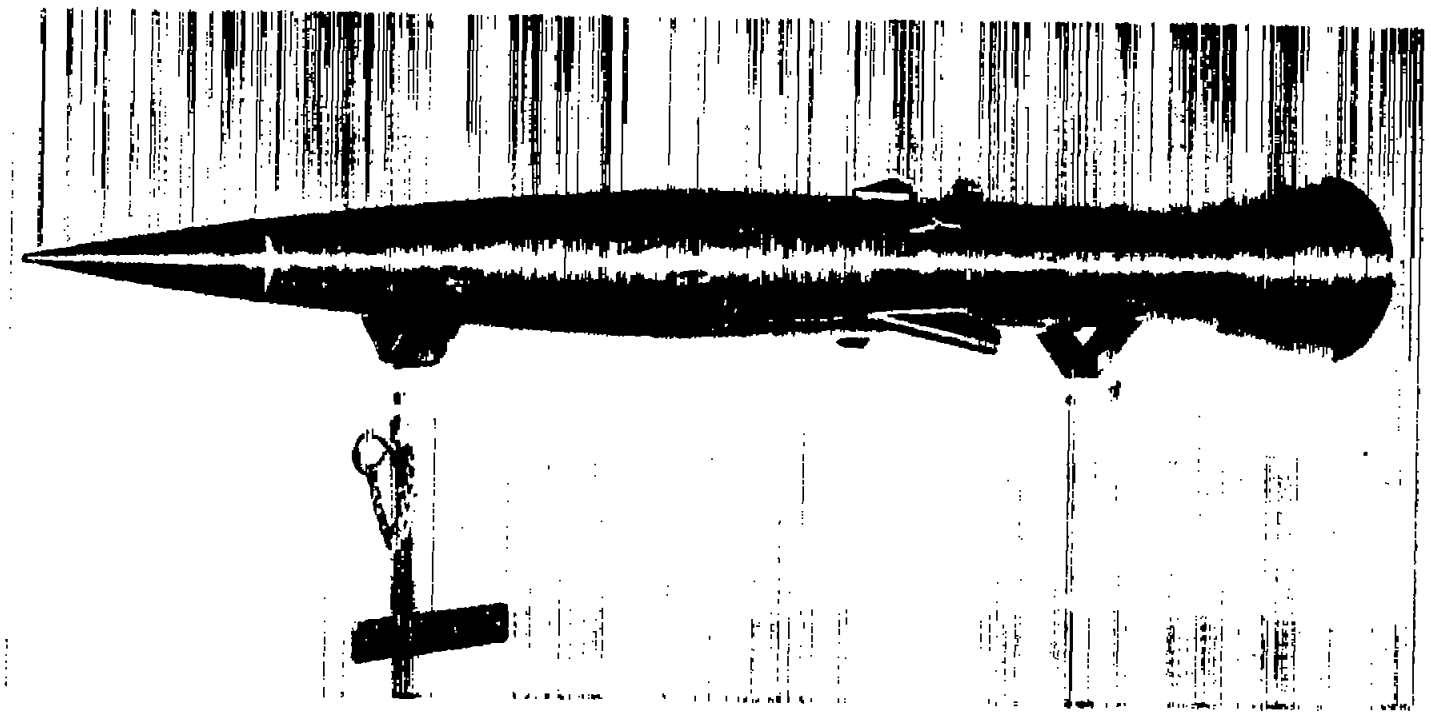

Figure 2.- Model used in the investigation. L-95260

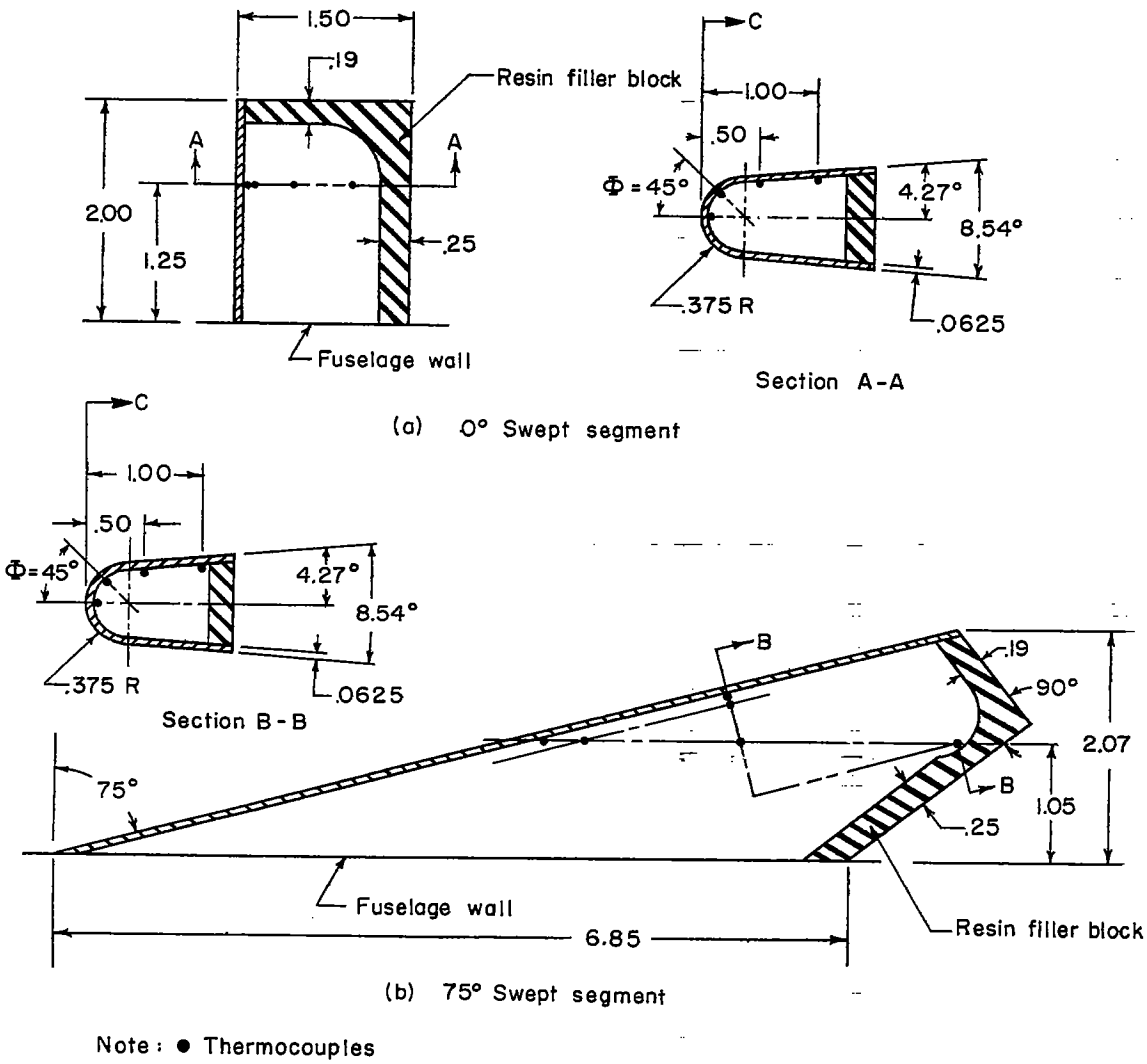

Figure 3.- Sketch of wing leading-edge segments showing thermocouple locations. All dimensions are in inches unless otherwise noted.

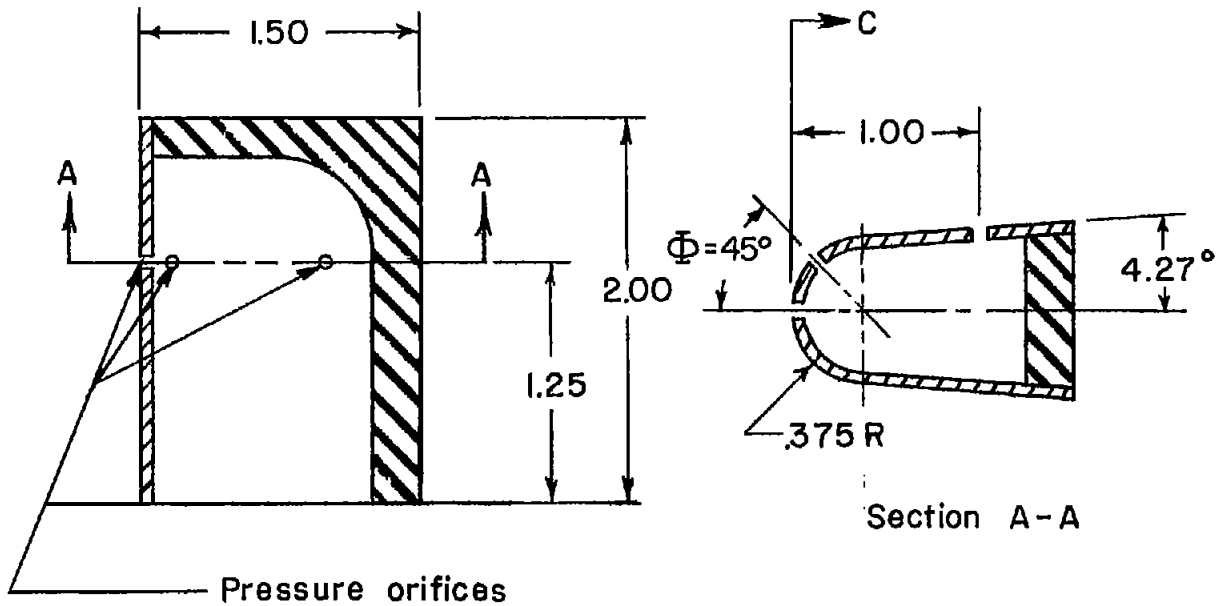

Figure 4.- Sketch of unswept-leading-edge segment showing pressure-orifice locations.

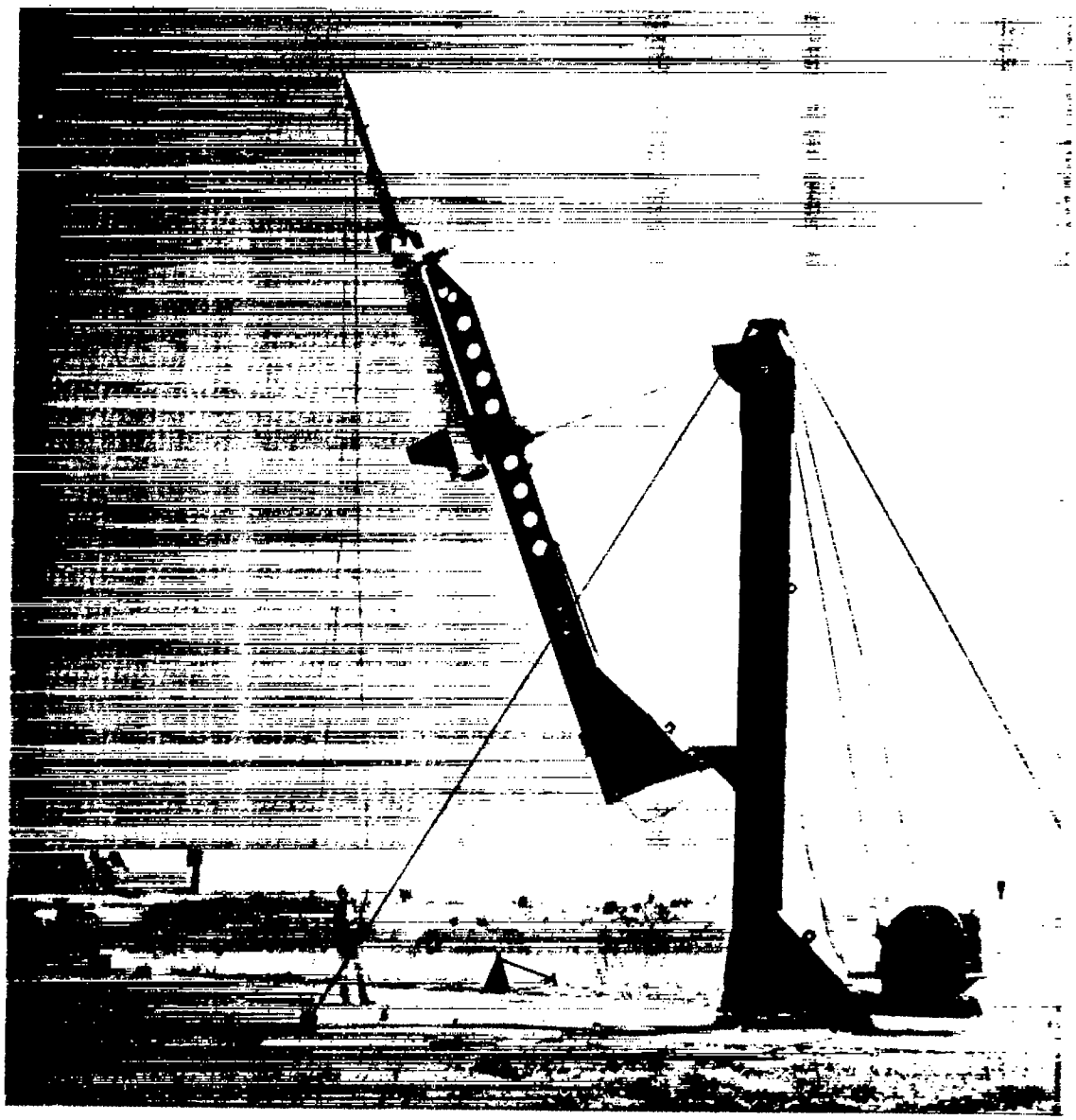

Figure 5.- Model and boosters on launcher. L-95364

[redacted]

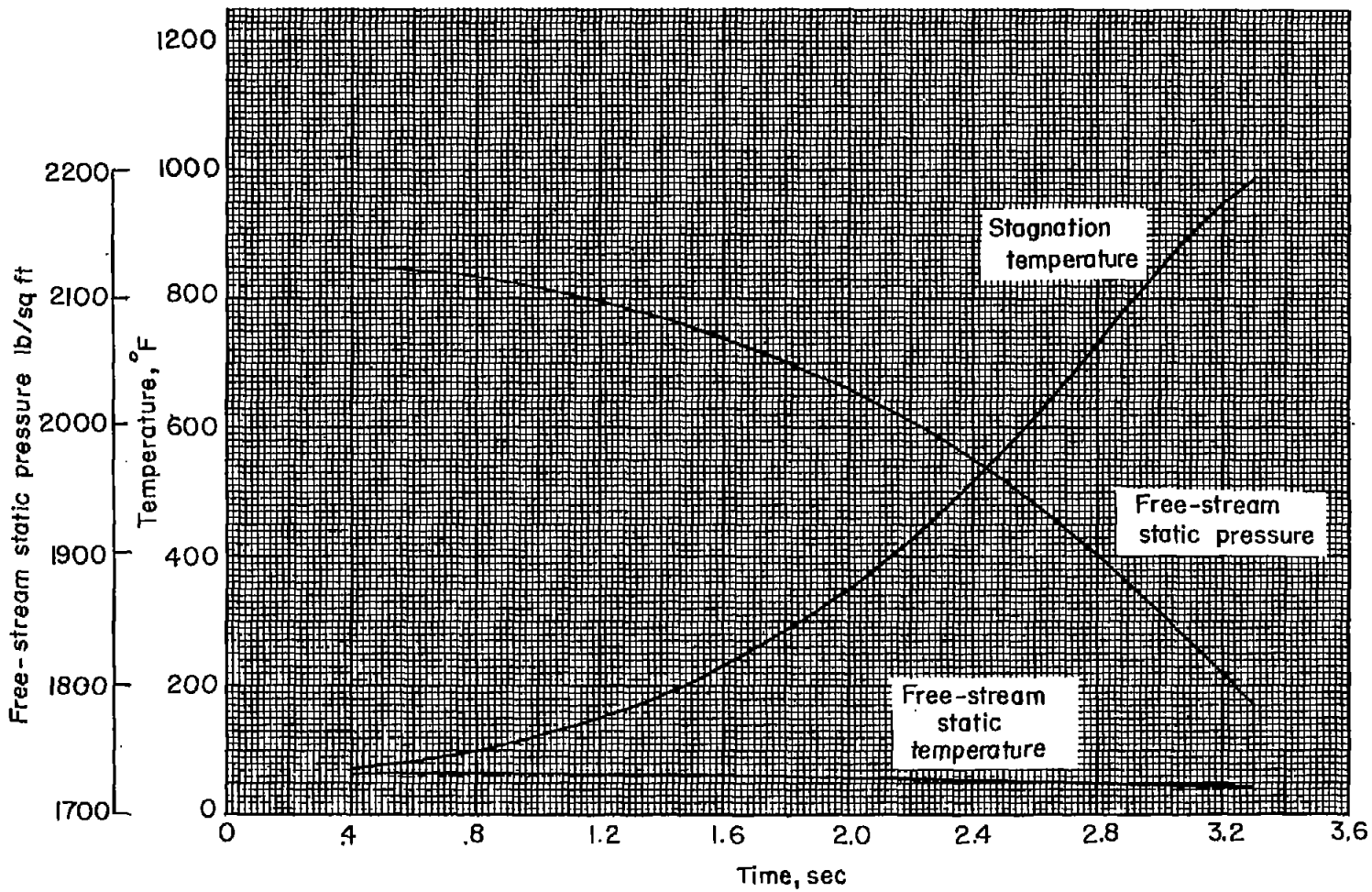

Figure 6.- Free-stream static temperature and pressure and stagnation temperature for model flight trajectory.

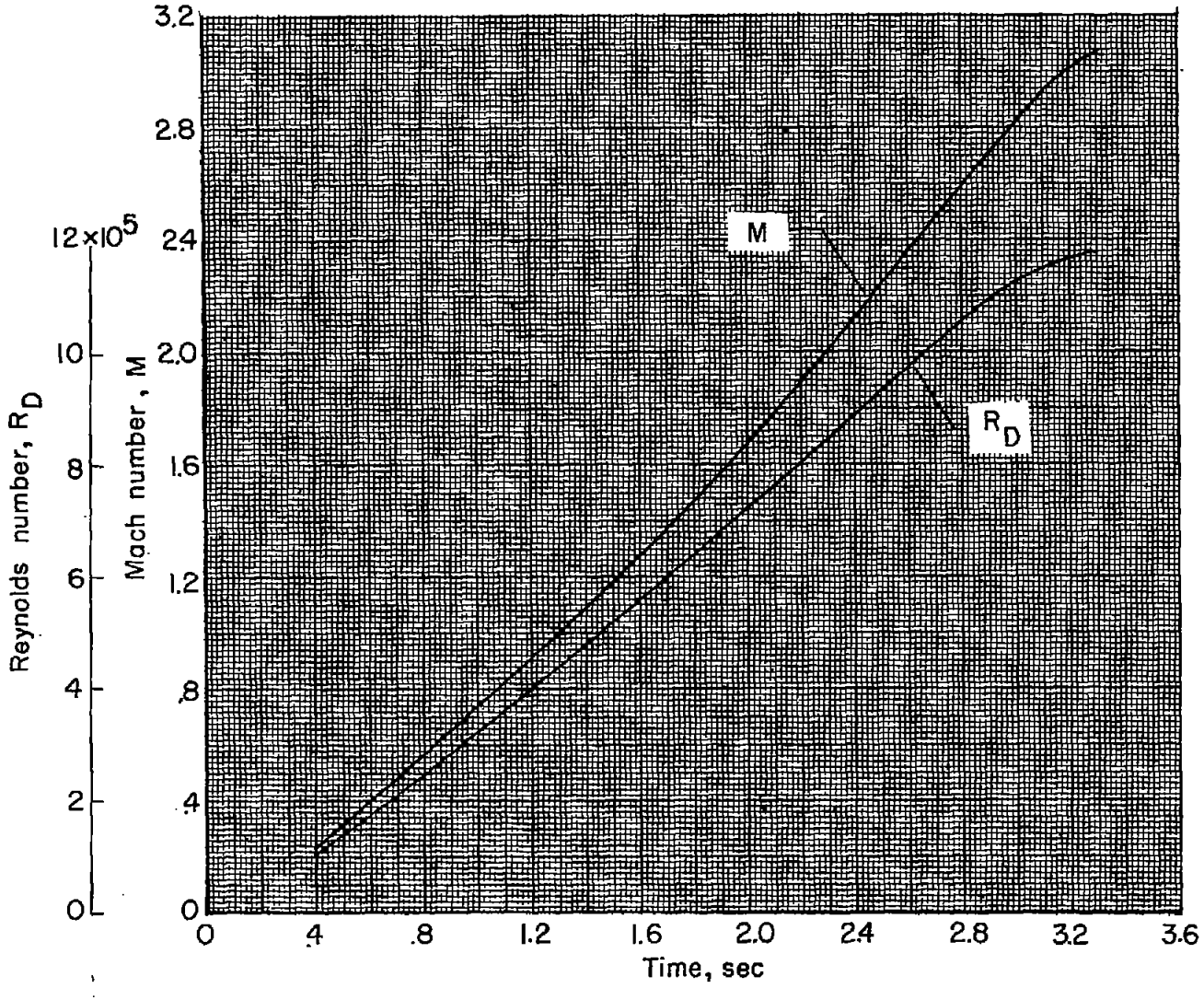

Figure 7.- Free-stream Mach number and Reynolds number (based on leading-edge diameter).

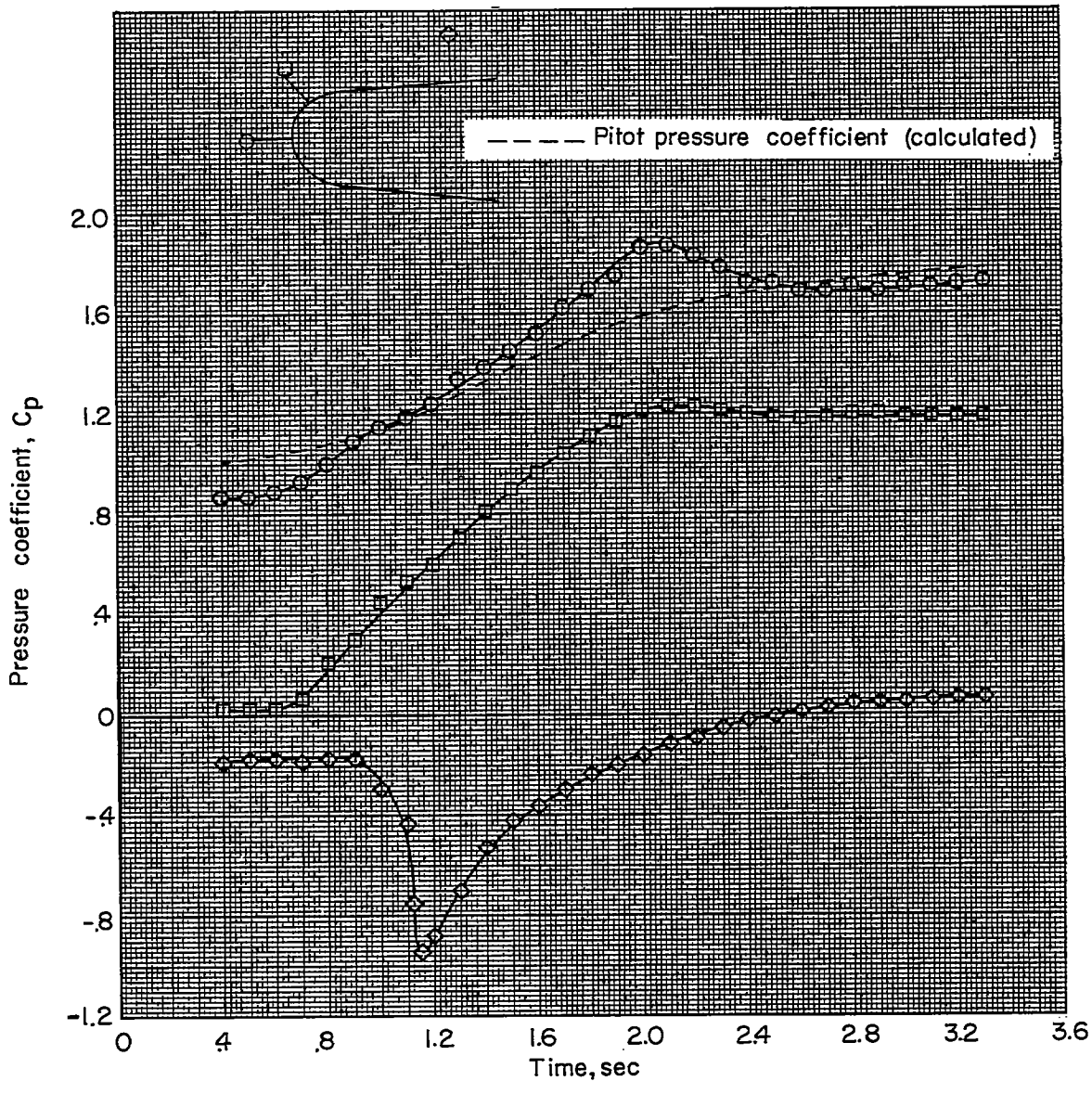

Figure 8.- Pressure coefficient for the unswept-leading-edge segment.

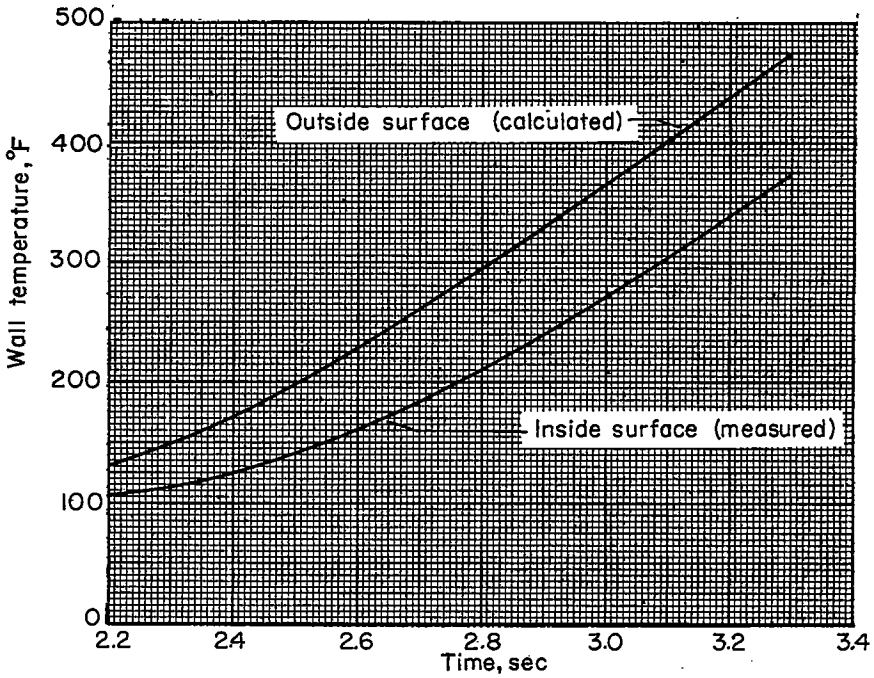

(a) Stagnation point, S/D = 0.

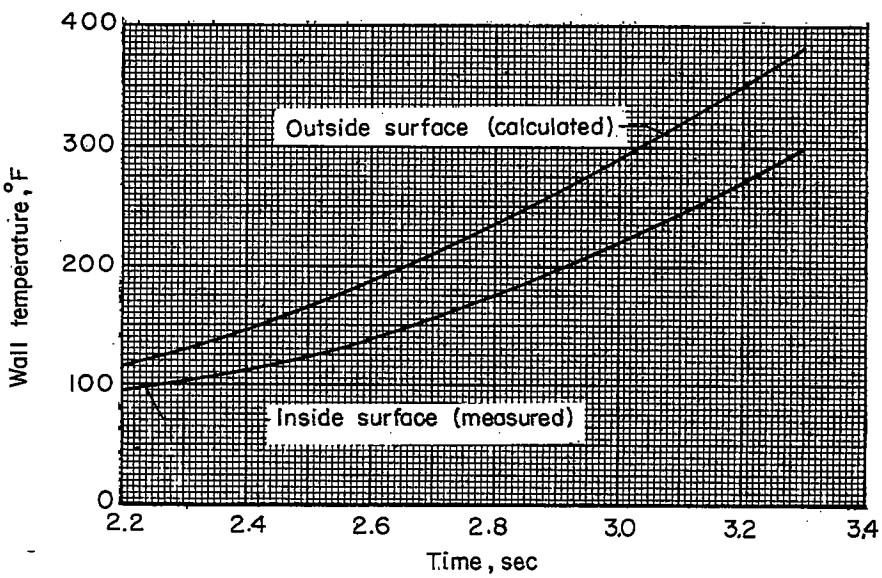

(b) $\Phi = 45^{\circ}$; S/D = 0.392.

Figure 9.- Unswept-leading-edge-segment temperatures.

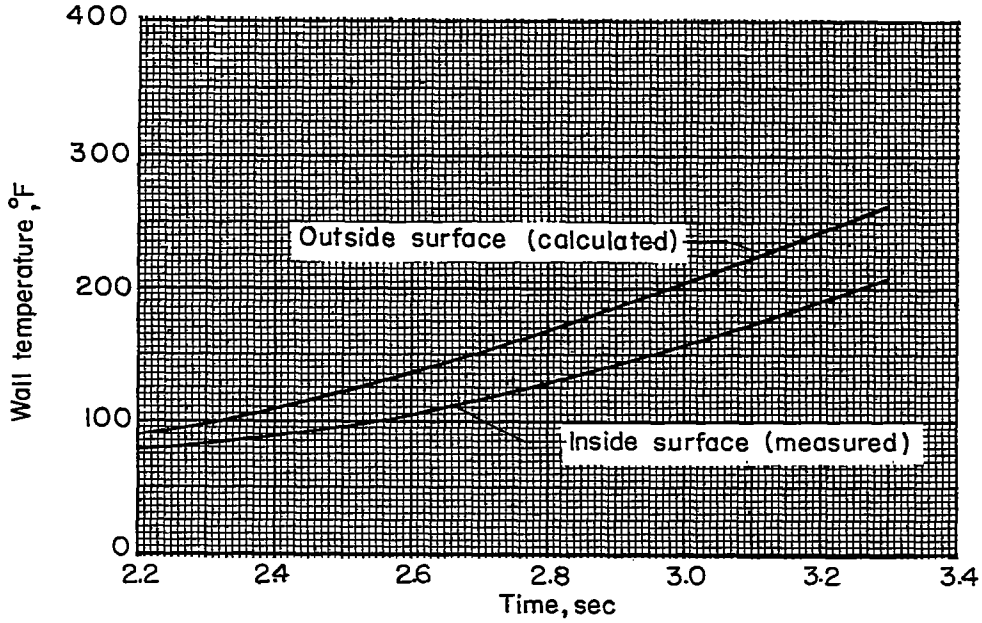

(c) C = 0.50 inch; S/D = 0.955.

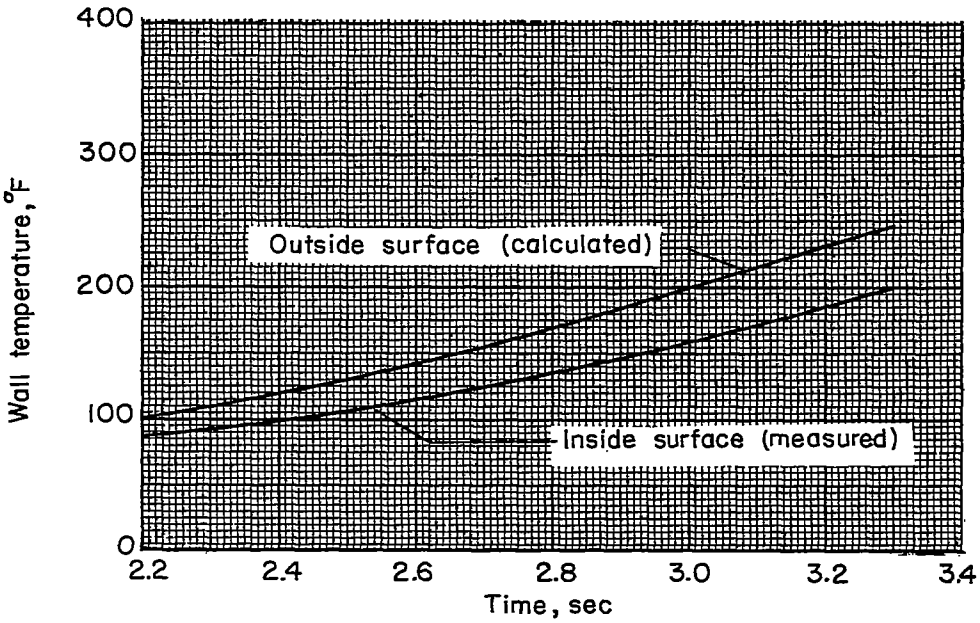

(d) C = 1.00 inch; S/D = 1.623.

Figure 9.- Concluded.

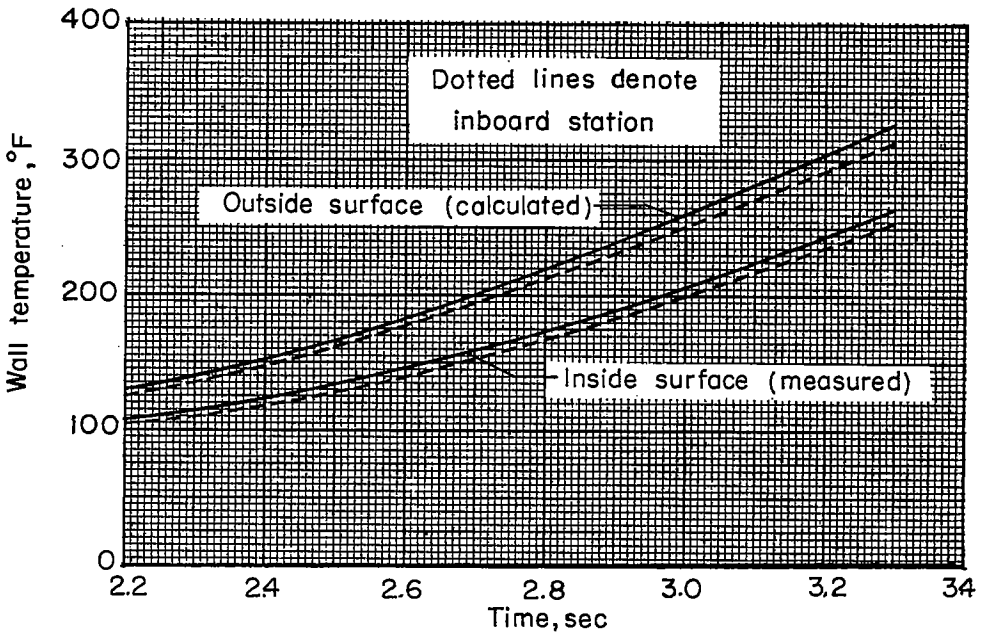

(a) Stagnation point, S/D = 0.

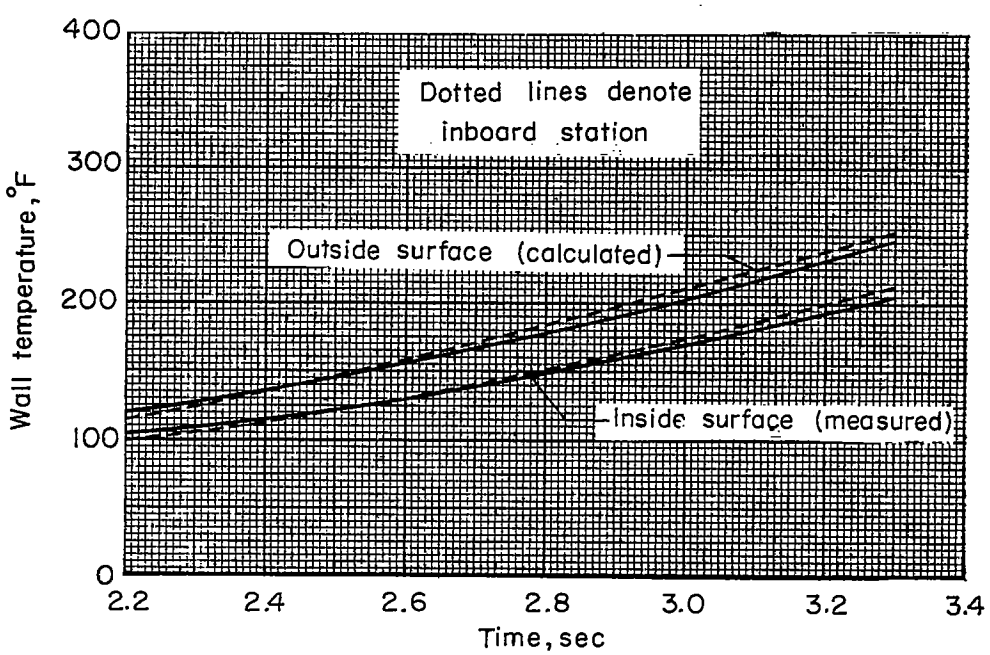

(b) $\Phi = 45^{\circ}$; S/D = 0.392.

Figure 10.- 75° swept-leading-edge-segment temperatures.

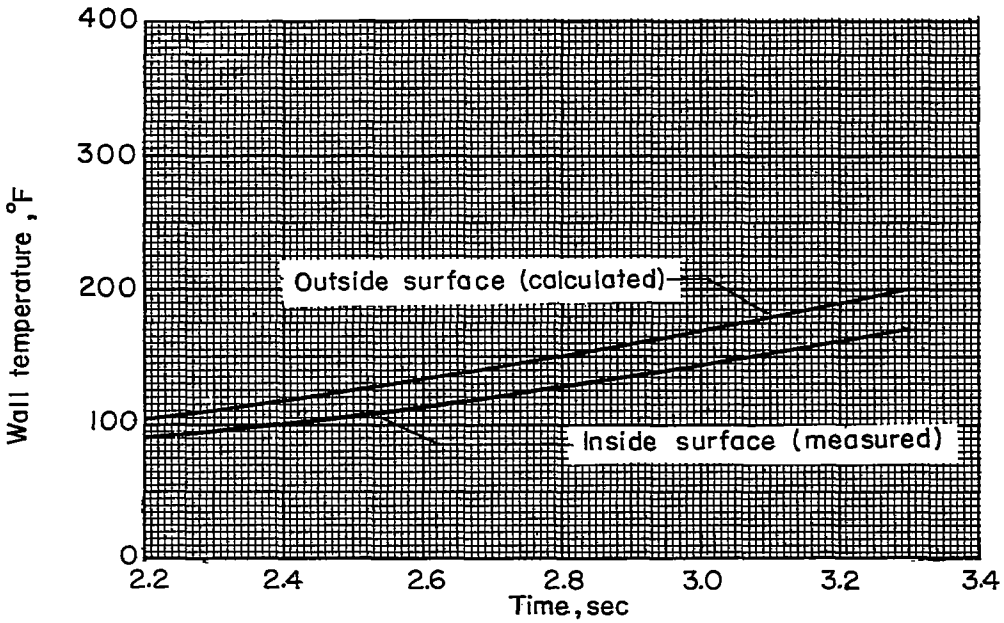

(c) C = 0.50 inch; S/D = 0.955.

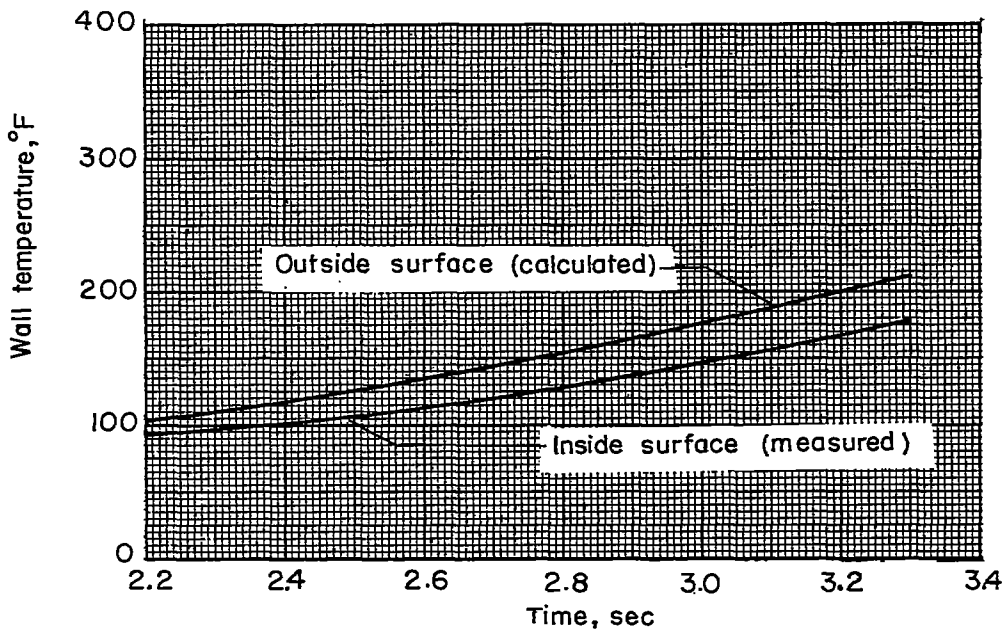

(d) C = 1.00 inch; S/D = 1.623.

Figure 10.- Concluded.

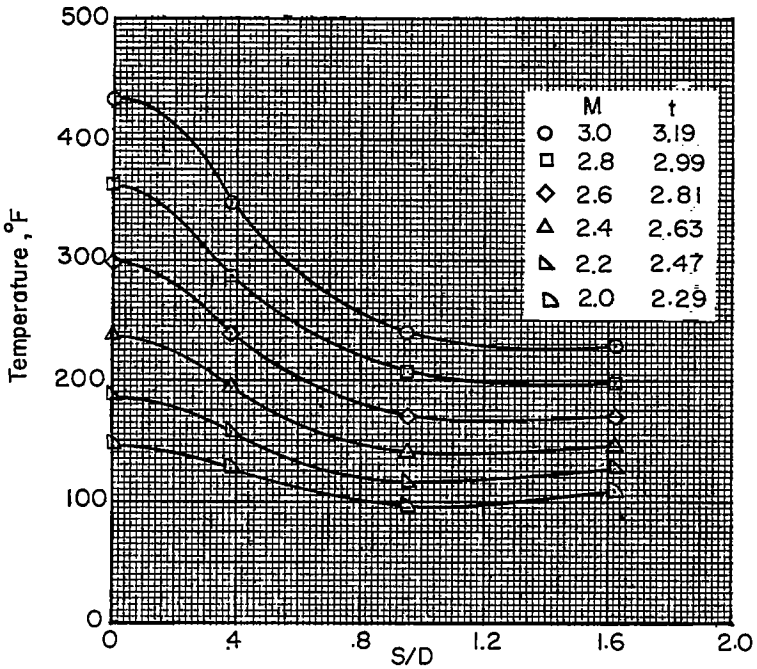

(a) $\Lambda = 0^{\circ}$.

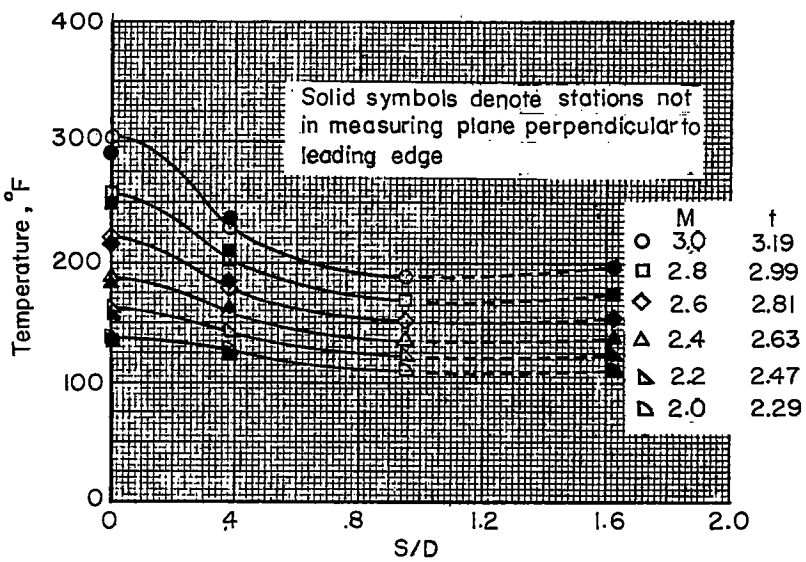

(b) $\Lambda = 75^{\circ}$.

Figure 11.- Chordwise distribution of outside-surface temperature.

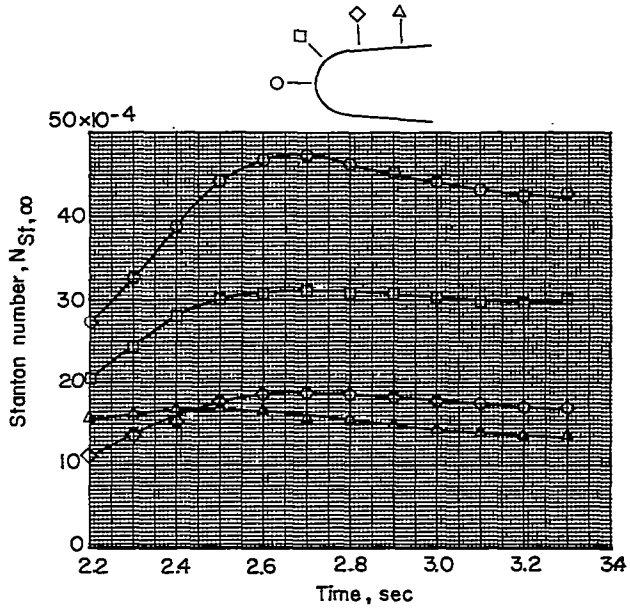

(a) $\Lambda = 0^{\circ}$.

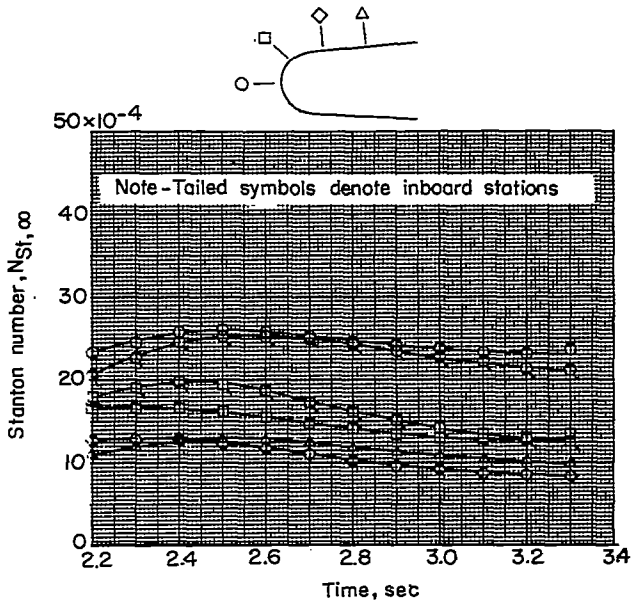

(b) $\Lambda = 75^{\circ}$.

Figure 12.- Measured Stanton number for both the 0° and 75° swept-leading-edge segments.

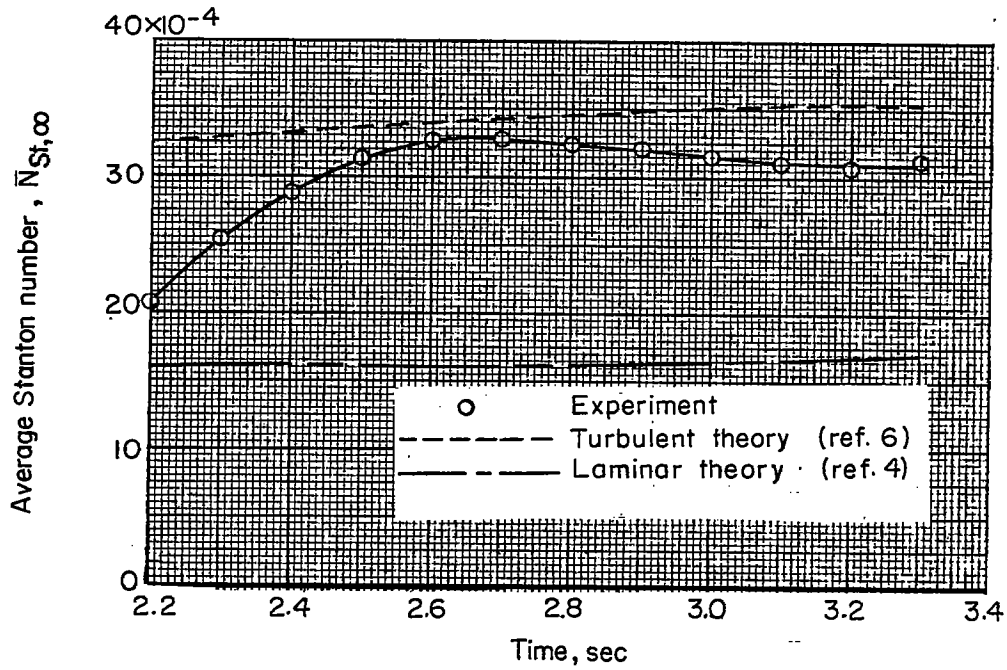

(a) $\Lambda = 0^{\circ}$.

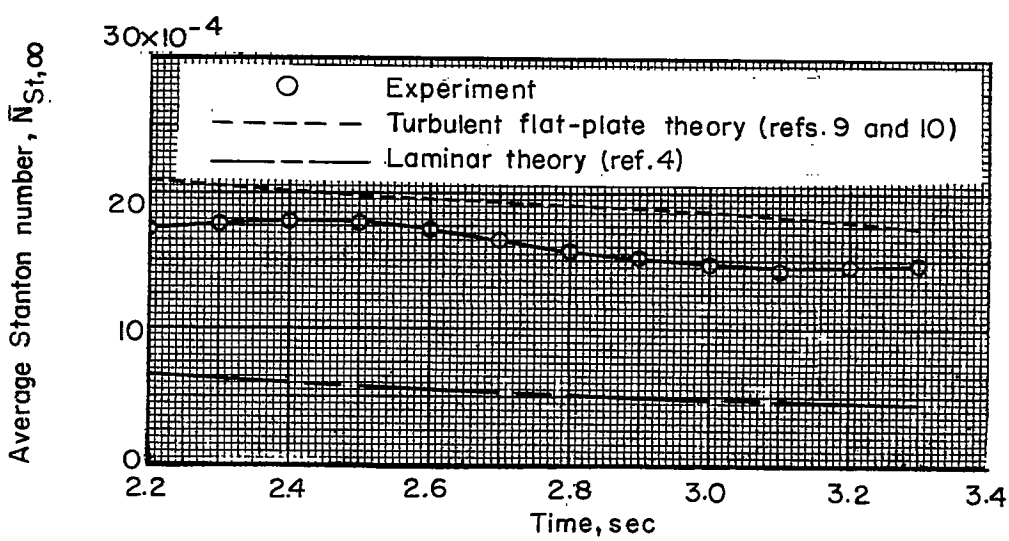

(b) $\Lambda = 75^{\circ}$.

Figure 13.- Comparison of experimental and theoretical Stanton numbers averaged around cylindrical portion of the 0° and 75° swept-leading-edge segments.

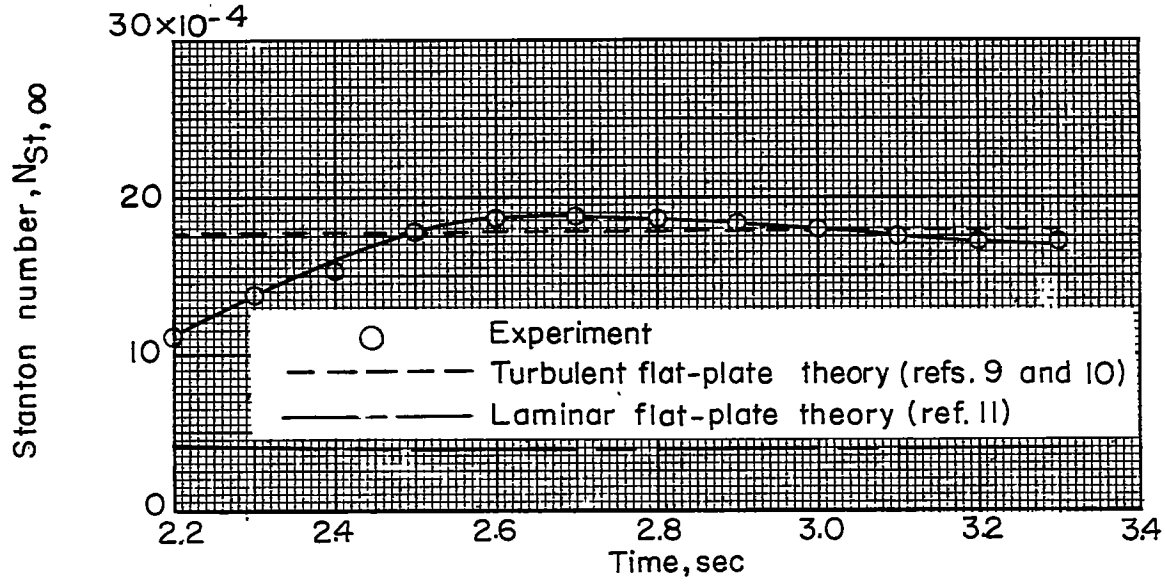

(a) $\Lambda = 0^{\circ}$; C = 0.50 inch.

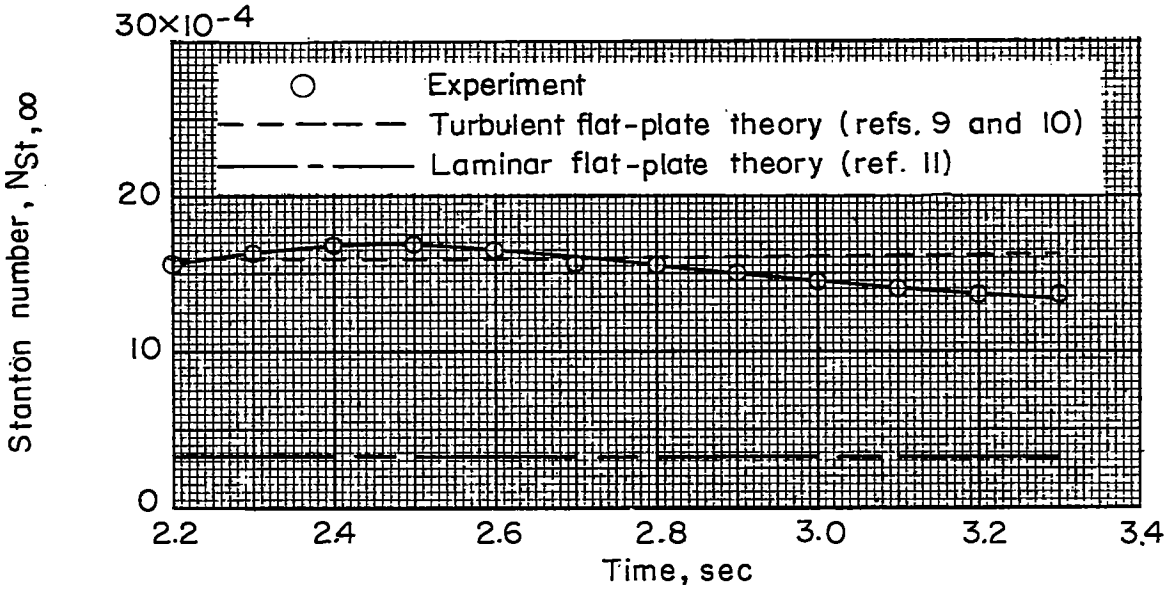

(b) $\Lambda = 0^{\circ}$; C = 1.00 inch.

Figure 14.- Comparison of experimental and theoretical Stanton numbers at two stations on the flat of the 0° and 75° swept-leading-edge segments.

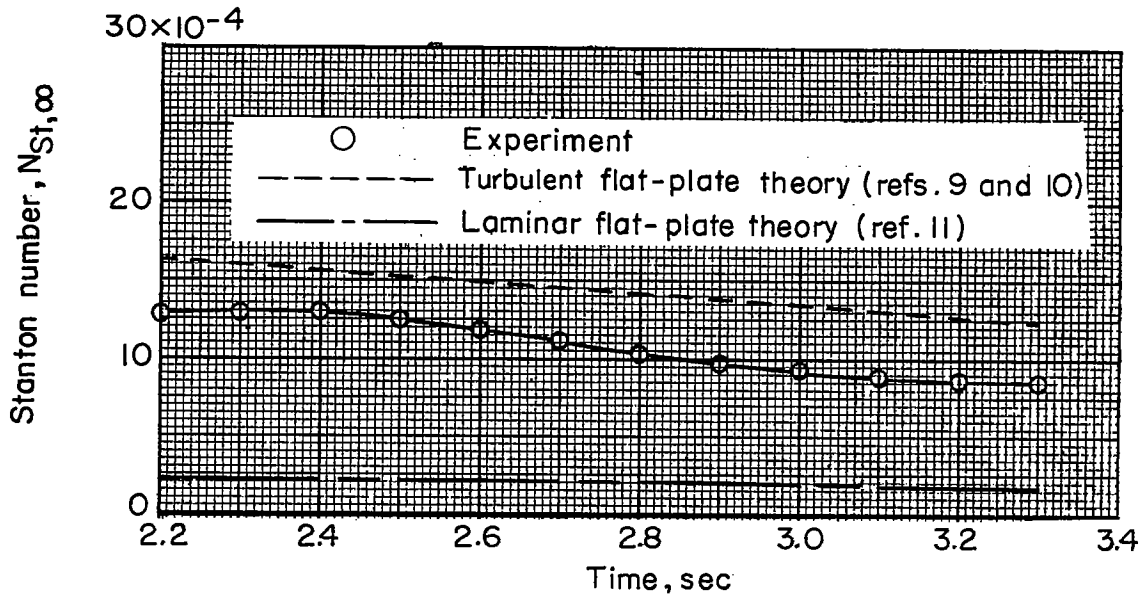

(c) $\Lambda = 75^{\circ}$; C = 0.50 inch.

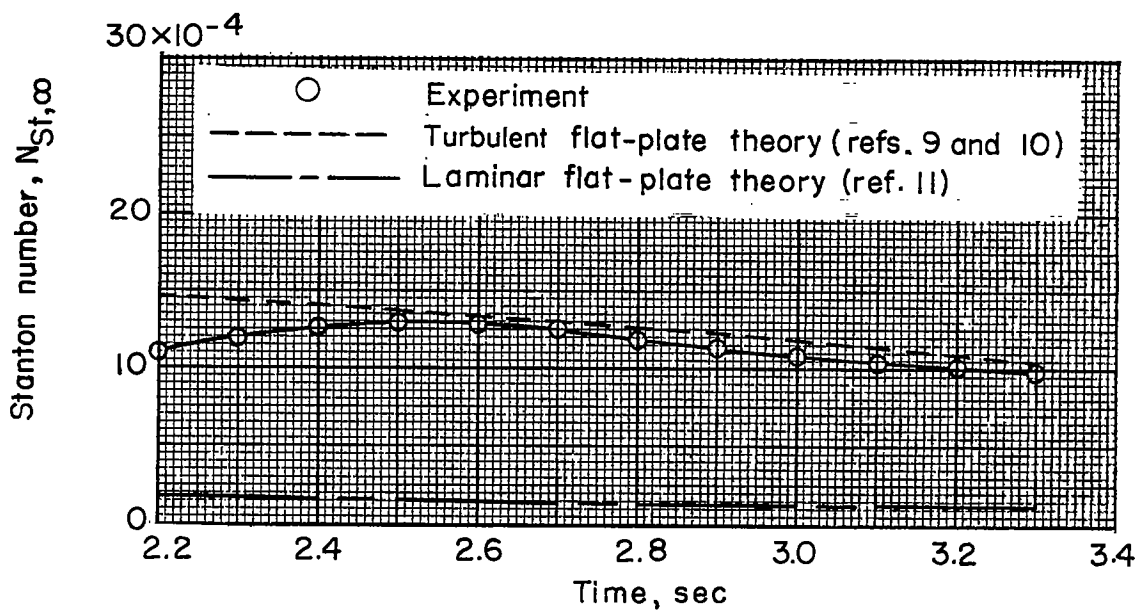

(d) $\Lambda = 75^{\circ}$; C = 1.00 inch.

Figure 14.- Concluded.

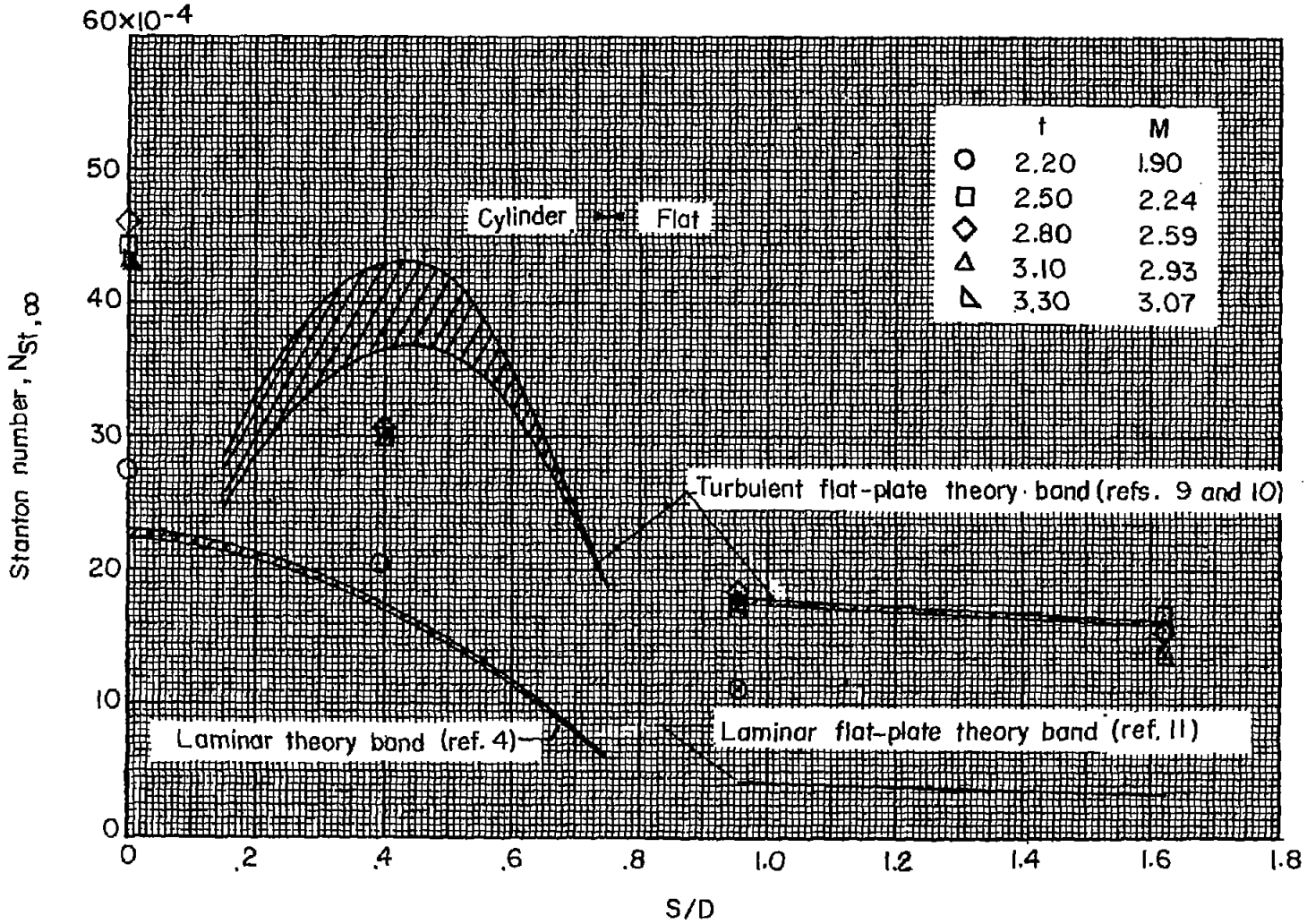

(a) $\Lambda = 0^{\circ}$.

Figure 15.- Comparison of experimental and theoretical Stanton numbers.

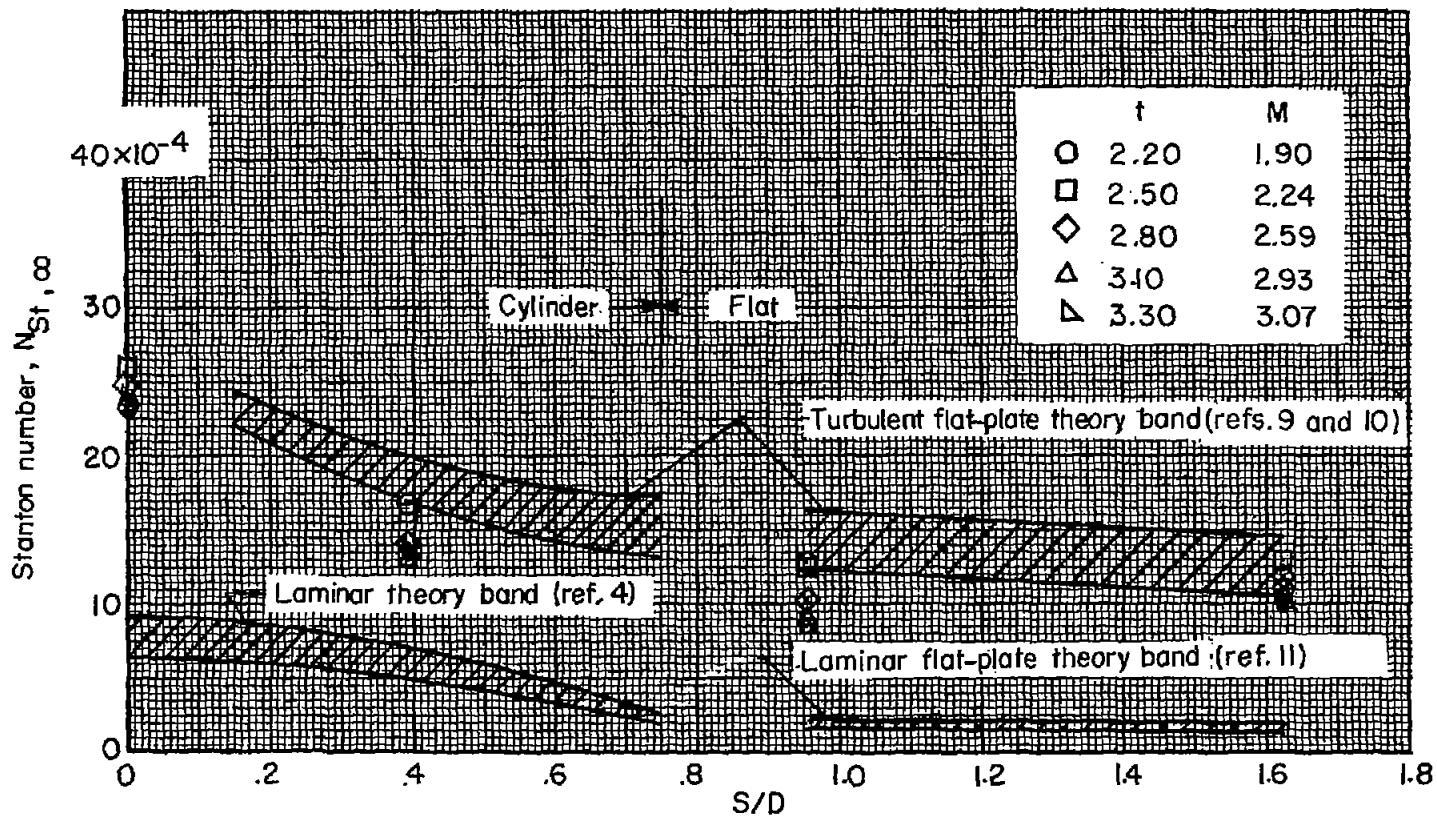

(b) $\Lambda = 75^{\circ}$.

Figure 15.- Concluded.